An Experimental Investigation of the Rossby Two-slit Problem

Alexis Kaminski

August 2014

1   Introduction

Rossby waves arise in the oceans as a response to forcing, either by buoyancy or by the actions of winds at the sea surface [3]. They have been observed in satellite altimeter data (for example, Kelly and Thompson (2002)[1] show excellent agreement between observed sea surface height and a Rossby wave model) as well as in moorings.

The case of Rossby waves in closed basins (i.e. Rossby basin modes) is a classical problem in geophysical fluid dynamics [2, 3, 4]. There is observational evidence from moorings for these modes; for example, Warren et al. (2002)[9] observed a large signal in moorings in the Mascarene Basin (off the coast of Madagascar) which they attributed to a barotropic Rossby mode.

When examining ocean circulation in basins with incomplete barriers, Pedlosky et al. (1997)[7] and Pedlosky and Spall (1999)[8] found that barriers extending through most of the ocean basin were surprisingly inefficient at blocking the transmission of Rossby wave energy from one subbasin to the next. Pedlosky (2000)[5] developed the linear theory further for the case of a long thin island extending nearly the entire meridional length of the basin, with only small gaps between the north and south ends of the island and the basin boundary, and found that for certain forcing symmetries, waves forced in the eastern subbasin were able to easily slip around the island into the western subbasin. Following this, Pedlosky (2001)[6] looked at the amplitude of reflected and transmitted waves through a barrier with two or three small gaps. However, the theory derived in Pedlosky (2000)[5] and Pedlosky (2001)[6] neglects nonlinear effects and friction in the main basin interiors, and it is unclear what effect these neglected processes will have. As such, investigation of this problem in a laboratory setting might be able to shed some light as to how well the linear theory captures the physics of Rossby waves impinging on a barrier with small gaps, such as ocean ridges or island chains with small gaps between neighbouring islands.

The remainder of this report will proceed as follows. In section 2, the details of the linear theory for the problem of Rossby modes interacting with a barrier with two gaps in it will be outlined, as well as giving a scaling for the likely impact of nonlinear effects. In section 3, the laboratory setup and the associated troubleshooting of the apparatus will be described. Then, in section 4, the measured flows will be described and compared with the linear theory. The quantitative details of the integral constraint derived in the linear theory will be examined using the laboratory data, and some effects of nonlinearity will be examined. We find that while the linear theory captures the large-scale structures of the flow as the Rossby modes encounter the barrier, viscosity and nonlinearity appear to significantly affect
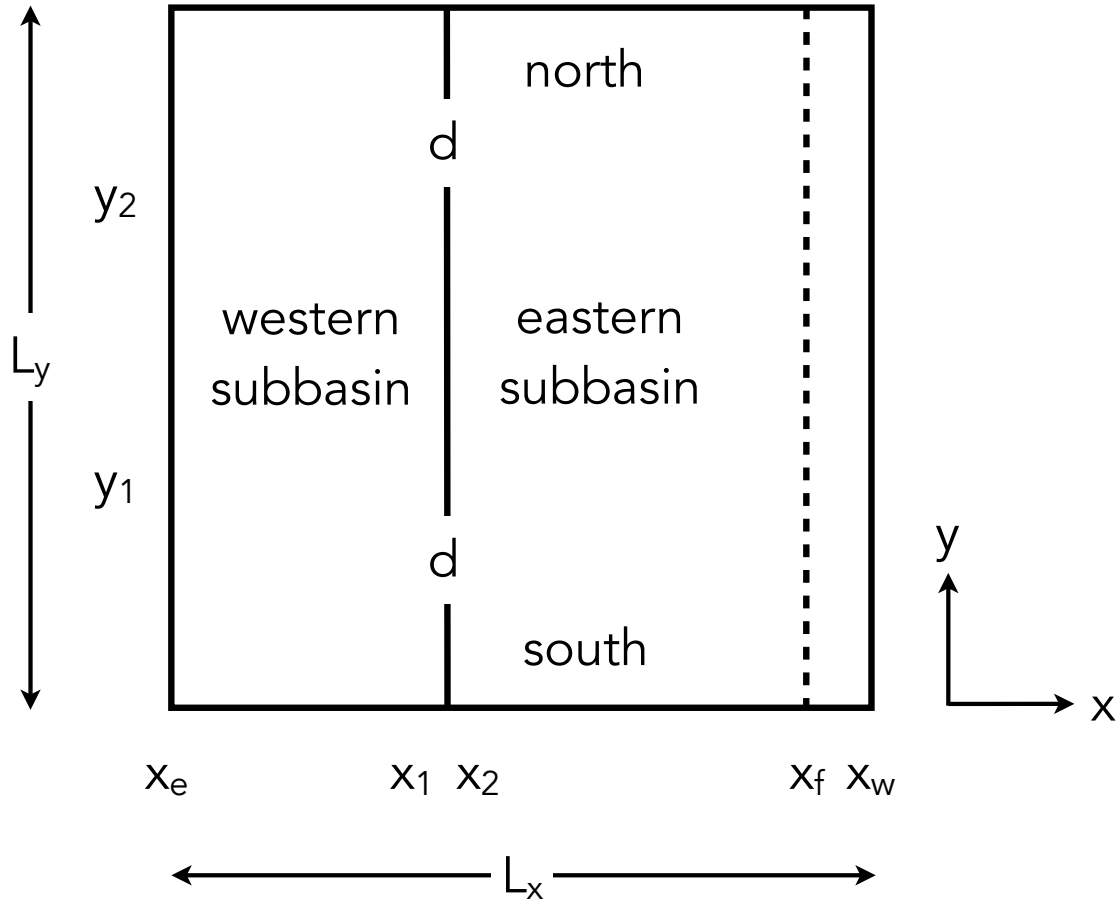
Figure 1: Geometry of basin, barrier, and forcing.

the flow along the boundaries and the barrier through strong boundary currents, and in the gaps through the formation of vortices. Additionally, there is no indication of resonance in the experimental results, despite the predicted resonance at the basin and subbasin normal mode frequencies in the linear theory, indicating additional missing physics. Finally, in section 5, future directions for the problem based on the laboratory results observed here will be discussed.

2   Linear theory

The geometry of the system being considered, shown in figure 1, is similar to that of Pedlosky (2001)[6]: a barrier from x_1 to x_2 extends the length of a square basin in the meridional direction with only two small gaps of length $d \ll L$, and is symmetric with respect to the y-coordinate. The flow is forced at the location $x = x_f$, similar to the forcing in Pedlosky (2000)[5].

As in Pedlosky (2000)[5], the governing equation for the flow is the linearized quasi-geostrophic potential vorticity equation for the β-plane. The fluid is homogeneous and the

flow is barotropic. In nondimensional form, with lengths scaled by the basin length L and times scaled by the characteristic Rossby wave period $(\beta L)^{-1}$, the equation of motion is

$$\nabla^2 \Psi_t + \Psi_x = -r\nabla^2 \Psi + A\nabla^4 \Psi + W(x,y,t)\,. \tag{1}$$

The first term on the right-hand side of (1), proportional to r, is a linear drag term representing the effect of bottom friction, and may be thought of as a ratio between Stommel's boundary layer thickness to L. The second term, proportional to the nondimensional viscosity A, represents the effect of lateral friction. It can be thought of as a cubed ratio of the Munk scale δ_M to L [5]. Both A and r are assumed to be small parameters. Finally, the third term is a forcing term.

As in Pedlosky (2000)[5], we assume that the forcing is harmonic with frequency ω_0,

$$W = \text{Re}[e^{i\omega_0 t} w(x,y)]\,. \tag{2}$$

We then search for solutions $\Psi(x,y,t)$ of the form

$$\Psi = \text{Re}[e^{i\omega_0 t} \psi(x,y)]\,. \tag{3}$$

Substituting the above expressions for W and Ψ into (1) thus leads to the following partial differential equation for the spatial structure of the stream function $\psi(x,y)$:

$$i\omega\nabla^2\psi + \psi_x = A\nabla^4\psi + w(x,y) \tag{4}$$

where $\omega = \omega_0 - ir$.

On the basin boundaries and the peninsulas, we set $\psi = 0$, while the island is assumed to have constant value Ψ_I, to be determined.

The vertical structure of the forcing may be represented as a Fourier sine series

$$w = \sum_{n=1}^{\infty} w_n(x)\sin n\pi y\,. \tag{5}$$

Additionally, if the forcing is localized in x, for instance at some location $x = x_f$, then the x-dependent coefficients $w_n(x)$ may be represented using a Dirac delta as

$$w_n = W_n\delta(x - x_f), \qquad x_2 < x_f < x\,. \tag{6}$$

2.1   Gaps

In the gaps, the characteristic length scales of the flow are assumed to be much smaller in the y-direction than in the x-direction. Correspondingly, x-derivatives are assumed to be negligible when compared with y-derivatives, and (4) becomes

$$i\omega\psi_{yy} - A\psi_{yyyy} = 0 \tag{7}$$

in the gaps.

Defining $y' = y_2 + d - y$ in the northern gap and $y' = y - y_1 + d$ in the southern gap, the solution to (7) is

$$\psi = A_1 + B_1\frac{y'}{d} + C_1\exp\left(\frac{(1+i)y'}{\delta}\right) + C_2\exp\left(\frac{-(1+i)y'}{\delta}\right)\,, \tag{8}$$

where $\delta = \sqrt{2A/\omega}$. The corresponding boundary conditions are that the streamfunction ψ be continuous across the gaps, i.e.

$$
\begin{aligned}
\psi &= 0, & y' &= 0, \\
\psi &= \Psi_I, & y' &= d, \\
\psi_y &= 0, & y' &= 0, d.
\end{aligned}
\tag{9}
$$

Applying (9) allows for the determination of the coefficients in (8) as

$$
A_1 = -\Psi_I \frac{\rho(1-q)}{(1+i)[1+q-\rho(1-i)(1-q)]}
\tag{10}
$$

$$
B_1 = \Psi_I \frac{(1+q)}{[1+q-\rho(1-i)(1-q)]}
\tag{11}
$$

$$
C_1 = -\Psi_I \frac{q\rho}{(1+i)[1+q-\rho(1-i)(1-q)]}
\tag{12}
$$

$$
C_2 = \Psi_I \frac{\rho}{(1+i)[1+q-\rho(1-i)(1-q)]}
\tag{13}
$$

with $\rho = \delta/d$ and $q = \exp(-(1+i)/\rho)$. The values of A_1, B_1, C_2, C_2 are proportional to Ψ_I which is yet to be determined.

Thus, the streamfunction along the longitudes of the barrier is

$$
\psi = \begin{cases}
0, & 0 < y < y_1 - d \\
\psi_{gap}, & y_1 - d < y < y_1 \\
\Psi_I, & y_1 < y < y_2 \\
\psi_{gap}, & y_2 < y < y_2 + d \\
0, & y_2 + d < y < 1
\end{cases}
\tag{14}
$$

which may be written as $\psi = \Psi_I g(y)$.

2.2   Basins

In the basin interior, lateral friction is neglected and (4) becomes

$$
i\omega \nabla^2 \psi + \psi_x = w(x, y).
\tag{15}
$$

The solution may be represented as

$$
\psi = e^{ikx} \sum_{n=1}^{\infty} \phi_n(x) \sin n\pi y,
\tag{16}
$$

so that solving for ψ amounts to solving

$$
\frac{d^2\phi_n}{dx^2} + a_n^2 \phi_n = \frac{w_n(x)}{i\omega} e^{-ikx},
\tag{17}
$$

in which $a_n^2 = k^2 - n^2\pi^2$ and $k = 1/(2\omega)$, for ϕ_n.

Solving (17) with the boundary conditions for ψ and continuity of the streamfunction at $x = x_f$,

$$\left.\frac{\mathrm{d}\phi_n}{\mathrm{d}x}\right|_{x=x_f+} - \left.\frac{\mathrm{d}\phi_n}{\mathrm{d}x}\right|_{x=x_f-} = -\frac{i}{\omega}W_n\mathrm{e}^{-ikx_f} \tag{18}$$

gives

$$\phi_n = \begin{cases} A_n^+ \frac{\sin a_n(x-x_e)}{\sin a_n(x_2-x_e)}, & x_f \leq x \leq x_e \\ A_n^- \frac{\sin a_n(x-x_e)}{\sin a_n(x_2-x_e)} + B_n \frac{\cos a_n(x-x_e)}{\sin a_n(x_2-x_e)}, & x_2 \leq x \leq x_f \\ D_n \frac{\sin a_n(x-x_w)}{\sin a_n(x_1-x_w)}, & x_w \leq x \leq x_1 \end{cases} \tag{19}$$

in which

$$B_n = \frac{W_n\mathrm{e}^{-ikx_f}}{i\omega a_n}\sin a_n(x_2 - x_e)\sin a_n(x_f - x_e) \tag{20}$$

$$A_n^- = \Psi_I g_n \mathrm{e}^{-ikx_2} - \frac{W_n\mathrm{e}^{-ikx_f}}{i\omega a_n}\cos a_n(x_2 - x_e)\sin a_n(x_f - x_e) \tag{21}$$

$$A_n^+ = A_n^- + B_n\cot a_n(x_f - x_e) \tag{22}$$

$$D_n = \Psi_I g_n \mathrm{e}^{-ikx_1} \tag{23}$$

In the above, g_n refers to the Fourier sine transform of $g(y)$,

$$g_n = 2\int_0^y g(y)\sin n\pi y\,\mathrm{d}y. \tag{24}$$

2.3 Integral constraint

To determine the value of Ψ_I, we may apply Kelvin's circulation theorem by integrating around a contour, C_I, bordering the island. This gives

$$\oint_{C_I} \mathbf{u}\cdot\mathrm{d}\mathbf{s} = 0 \tag{25}$$

for time-periodic motion with frequency ω. This may be expressed as

$$i\omega\oint_{C_I}\nabla\psi\cdot\mathrm{n}\,\mathrm{d}l - A\oint_{C_I}\nabla\nabla^2\psi\cdot\mathbf{n}\,\mathrm{d}l = 0. \tag{26}$$

When the above expressions for ψ are substituted into the above, the resulting algebraic expression is for this integral constraint is

$$\Psi_I\left[\sum_{n=1}\frac{\mu_n g_n a_n\cos n\pi y_1}{n\pi}\frac{\sin a_n[L_x - l_x]}{\sin a_n(x_2 - x_e)\sin a_n(x_1 - x_w)} - \frac{2B_1 l_x}{d}\right]$$
$$= -i\sum_{n=1}\frac{\mu_n W_n\cos n\pi y_1}{\omega n\pi}\exp ik(x_2 - x_f)\frac{\sin a_n(x_f - x_e)}{\sin a_n(x_2 - x_e)} \tag{27}$$

where $\mu_n = 1 - (-1)^n$. This may then be solved for the island constant Ψ_I.

It should be noted that when n is even, the resulting value of Ψ_I is identically zero. This may be understood by considering that for the symmetric island geometry described

here, the integral around the island may be satisfied on the eastern side of the island alone: the meridional velocities along the eastern side integrate to zero.

However, when n is odd, $\Psi_I \neq 0$ in general. In contrast to the even-n case, the velocities along the eastern side of the island do not integrate to zero. This requires some response on the western side of the island in order to satisfy the integral constraint.

Finally, it should be noted that within the theoretical framework considered here, the result for the integral constraint is also applicable to the nonlinear equations of motion, i.e. integration around the island would still imply some response on the western side of the island to satisfy the integral constraint.

2.4 Scaling for nonlinearity

While the theory presented above is a linearized theory for the problem being considered, in a real fluid it is expected that nonlinear effects may become important in certain flow regimes. By considering the relative importance of the nonlinear terms in the full nonlinear quasigeostrophic potential vorticity equation, we can predict under what circumstances nonlinear effects may become important.

We begin by defining a characteristic forcing velocity $U_e = \omega_0 A_{\text{forcing}}$. Then, the (dimensional) stream function in the basin is expected to scale with this forcing velocity as $\psi_e \sim U_e L$. In addition, x distances are expected to scale roughly with L everywhere. In the basin, y distances scale approximately with L. We can then define a parameter NL_{basin} as a scaling of the relative importance of the nonlinear $J(\psi, \nabla^2 \psi)$ terms compared with the linear $\beta \psi_x$ term, i.e.

$$\frac{J(\psi, \nabla^2 \psi)}{\beta \psi_x} \sim \frac{U_e}{\beta L^2} = NL_{\text{basin}} . \tag{28}$$

However, in the gaps the y distances do not scale with L, but rather with d. A similar parameter NL_{gap} can thus be defined as

$$\frac{J(\psi, \nabla^2 \psi)}{\beta \psi_x} \sim \frac{U_e L}{\beta d^3} = NL_{\text{gap}} . \tag{29}$$

For gaps which are small compared with the length of the barrier, $d \ll L$, this implies that $NL_{\text{gap}} \gg NL_{\text{basin}}$, i.e. nonlinear effects are expected to be more significant in the gaps than in the basin interior.

3 Laboratory setup

The general experimental setup is shown in figure 2, with the corresponding parameters listed in table 1. The resulting laboratory apparatus is shown in figure 3, and consists of a square tank with a sloping bottom on a rotating table to create a laboratory analogue to the β-effect. A meridional barrier, constructed from $1/8''$ acrylic, is placed in the tank; the geometry of the barrier is symmetric with respect to y. The 45 cm-long forcing paddle is mechanically forced by a scotch yoke-type mechanism which allows for different forcing frequencies ($\mathcal{O}(0.10)\,\text{rad/s}$) and amplitudes (up to 3 cm). A rigid lid is used in order to reduce surface gravity-capillary modes in the system.
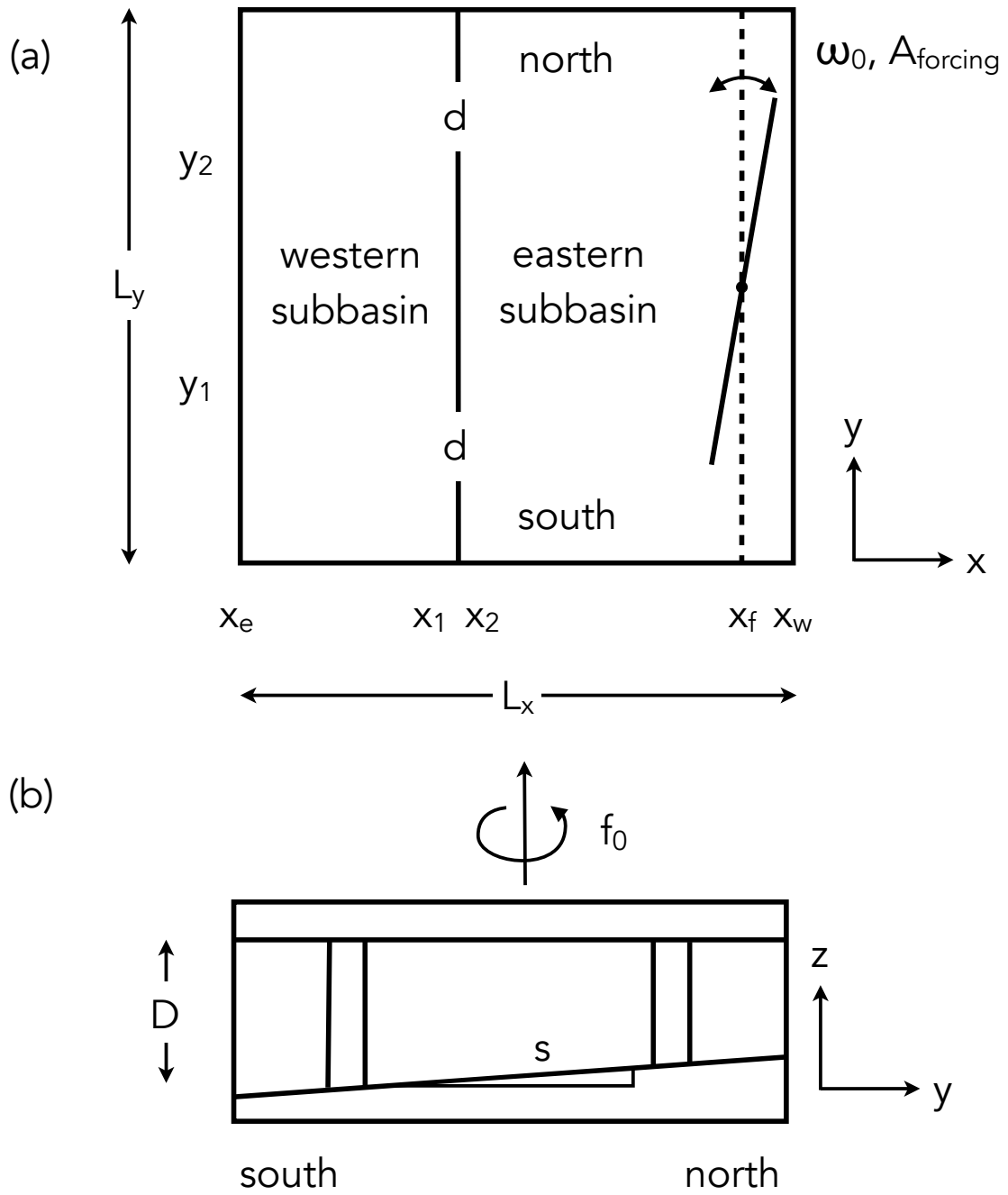
Figure 2: Geometry of basin, barrier, and forcing for laboratory experiments. (a) xy-plane. (b) yz-plane.

Parameter	Value	Parameter	Value
L_x	60 cm	y_1	15 cm
L_y	60 cm	y_2	45 cm
d	4 cm	D	20 cm
x_w	0 cm	s	2/15
x_e	60 cm	A_{forcing}	0.7-3.0 cm
x_1	22 cm	ω_0	0.05-0.15 rad/s
$x_2 - x_1$	$1/8''$	f_0	2.0-3.5 rad/s
x_f	57 cm		

Table 1: Experimental parameters used in laboratory experiments, corresponding to figure 2.

Two types of experiments are performed: dye visualization and particle image velocimetry (PIV). For the dye experiments, a syringe pump capable of low flow rates ($\mathcal{O}(1\,\text{ml/hr})$) is used to inject dye at various locations within the basin. For the PIV experiments, salt-water with density $\rho \approx 1200\,\text{kg/m}^{-3}$ is used as the working fluid. The fluid is seeded with $50\,\mu$ particles with density $\rho \approx 1160\,\text{kg/m}^{-3}$. A green laser ($532\,\text{nm}/1064\,\text{nm}$) is used to illuminate the flow, with a pulse rate of 1-10 Hz. The software used to compute the flow velocities is LaVision's DaVis software.

The Ekman layer depth, relative to the change in depth due to the sloping bottom, is $\delta_{Ek}/\Delta D \sim 0.01 - 0.02$. The Munk scale, relative to the gap width, is $\delta_M/d < 0.25$ (where the gap needs to be at least twice the Munk scale, to prevent the boundary layers from blocking flow through the gap). Given that $d \ll L$, this confirms the assumption in § 2 that A is a small parameter.

We anticipate a resonant response at approximately the normal-mode frequencies associated with the full basin in the absence of the barrier as well as those for each individual subbasin [8, 5]. These frequencies are computed in nondimensional form (relative to $(\beta L) \sim 1$) by

$$\omega_{nm} = \frac{1}{2\pi\sqrt{m^2(L_y/L_x)^2 + n^2}}, \tag{30}$$

in which the integers m and n refer to the mode number in the x and y directions, respectively [3]. These frequencies are $\omega_F = 0.1075$, $\omega_E = 0.0802$, and $\omega_W = 0.0548$ for the full, eastern, and western basins respectively.

4 Results

4.1 Initial results and troubleshooting

Initial dye visualization experiments (not shown) showed evidence of oscillations at approximately the forcing frequency. However, one limitation of the dye visualization technique is that it only gives a Lagrangian description of particle paths, and not a full picture of the overall flow field, which motivated the move to full PIV measurements of the flow.

Figure 3: Laboratory apparatus corresponding to figure 2.

However, upon taking initial PIV measurements of the flow, a high-frequency oscillation of $\mathcal{O}(1\,\text{Hz})$ was observed with amplitude comparable to that of the signal being forced. The high-frequency signal persisted even when the forcing was turned off entirely, as shown in figure 4; as such, it was necessary to determine the cause of the oscillations in order to reduce or eliminate them.

Several possible sources of oscillations were examined:

1. Surface gravity waves.
   Although a rigid lid for the tank is included in the experimental apparatus, it seemed possible that the lid may have still been able to wobble, thus forcing a flow in the interior of the tank. However, sealing down the lid did not appear to reduce the observed oscillations.

2. Table off-balance.
   Given the addition of the camera, camera mount, and laser to the table, it was thought that perhaps the weight may have unbalanced the table surface. However, adding weight to the opposite side of the table to offset this potential imbalance did not appear to reduce the oscillations.

3. Table not level.
   It was found that the table was not properly level, i.e. the axis of rotation was not parallel to gravity. Re-levelling the table appeared to help slightly but did not substantially reduce the oscillations.

4. Additional vibration introduced by control system.
   Due to the setup of the control system used to maintain the table's rotation speed, a peak in frequency of $\mathcal{O}(1\,Hz)$ could be observed in the associated frequency spectrum. By changing the manner in which the table was operated, the oscillations observed within the tank were reduced significantly.

With the oscillations observed in figure 4 substantially reduced, the PIV measurements of the forced flow could then be measured.

4.2 Comparison of PIV results with linear theory

PIV experiments were carried out at five forcing frequencies ($\omega_0 = 0.0690, 0.0882, 0.1010, 0.1134, 0.1355\,\text{rad/s}$) and three forcing amplitudes ($A_{\text{forcing}} = 0.7, 2.0, 2.7\,\text{cm}$) with a table rotation rate of $15\,\text{rpm}$ ($f_0 = 3.1\,\text{rad/s}$).

Figures 5 and 6 show the stream functions and velocities, respectively, from the laboratory measurements and the corresponding linear theory for forcing with $\omega_0 = \omega_F = 0.1355\,\text{rad/s}$ (at $f_0 = 3.1\,\text{rad/s}$) and $A_{\text{forcing}} = 2.0\,\text{cm}$. As the two figures show, despite the noise apparent in the experimental data, the linear theory does capture many of the large-scale features of the observed flow from the experiments. In particular, the computed streamfunction shown in figure 5 shows the Rossby wave propagating through the barrier with the correct frequency, as predicted by the linear theory.

Using the computed streamfunction from the experimental data, the experimental island constant can be computed. This is done by taking the average value of the streamfunction
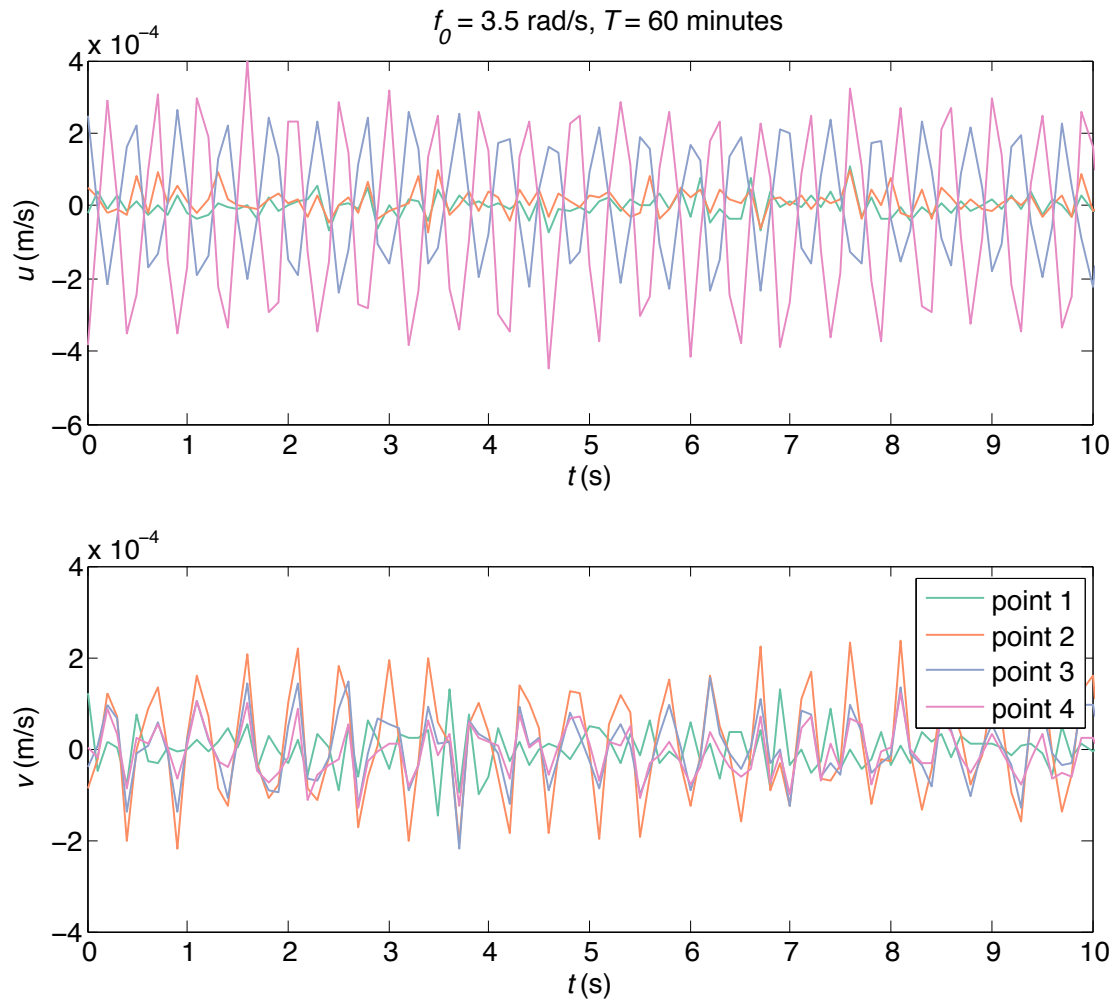
Figure 4: Horizontal (top) and vertical (bottom) velocities at four points in basin. Points 1, 2, 3, and 4 correspond to the northern gap, southern gap, centre of the western subbasin, and centre of the eastern subbasin, respectively.
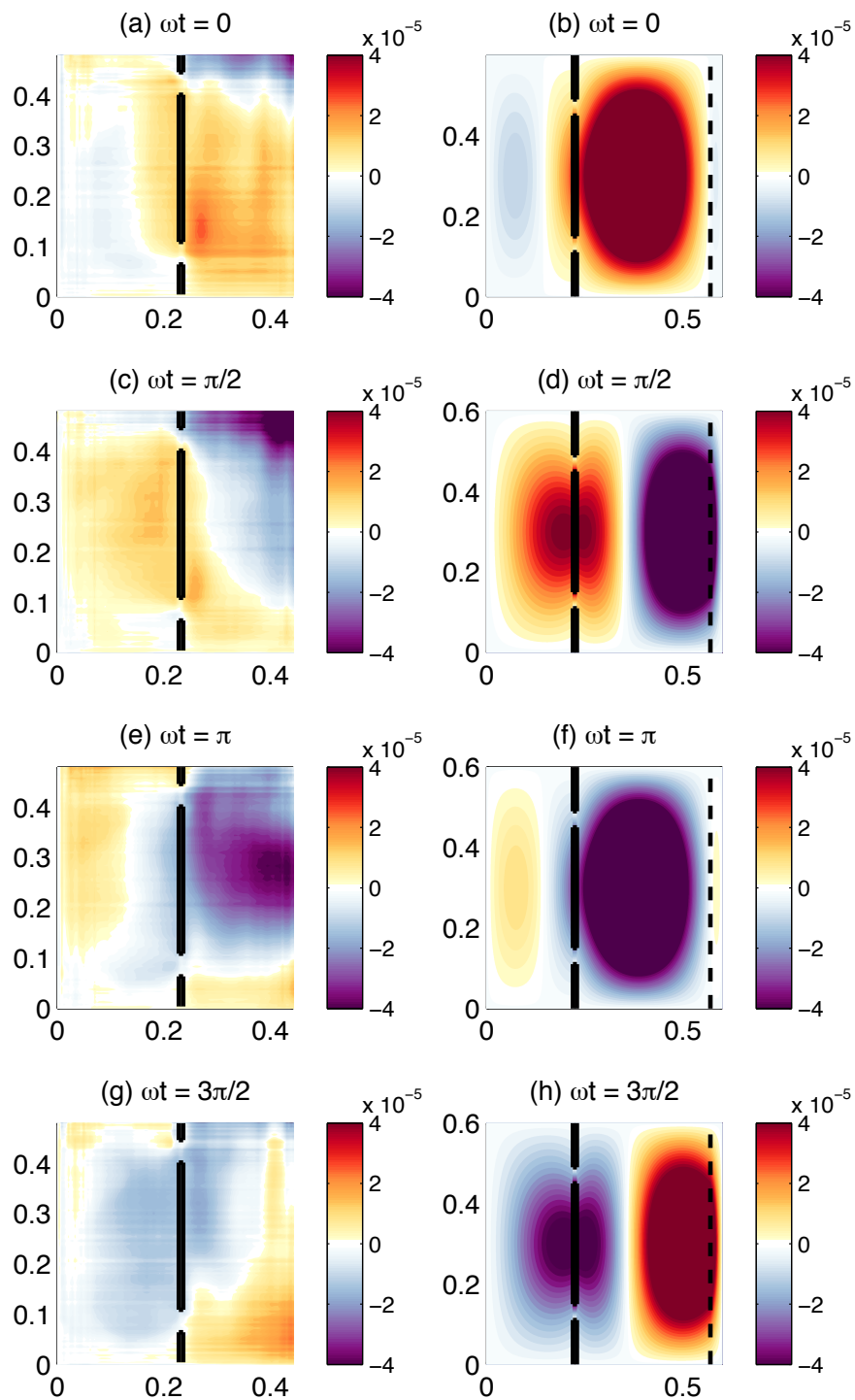
Figure 5: Comparison of streamfunction in laboratory results (left) and theoretical model (right) for $\omega_0 = \omega_F = 0.1355 \, \text{rad/s}$ at $f_0 = 3.1 \, \text{rad/s}$ and $A_{\text{forcing}} = 2.0 \, \text{cm}$.
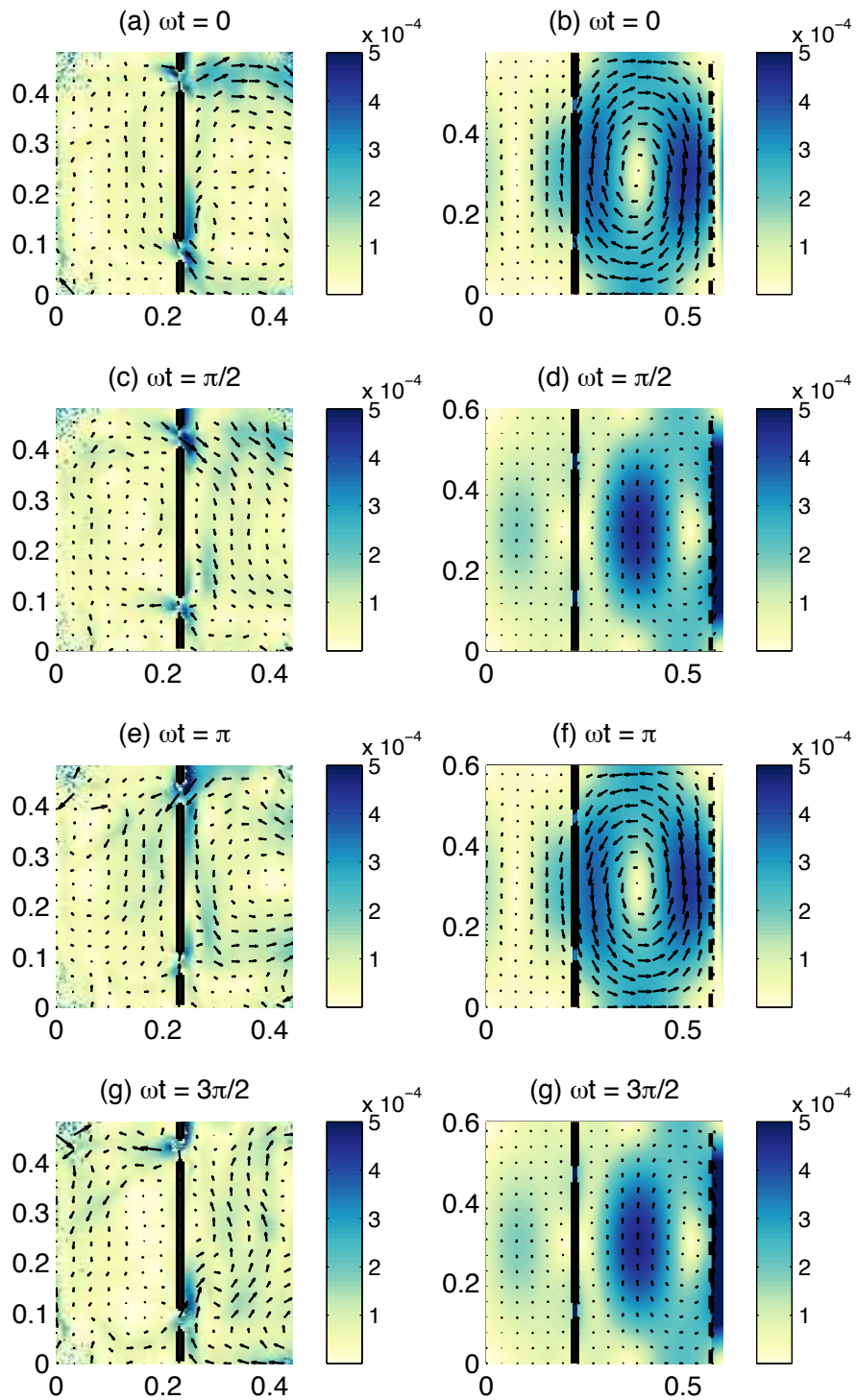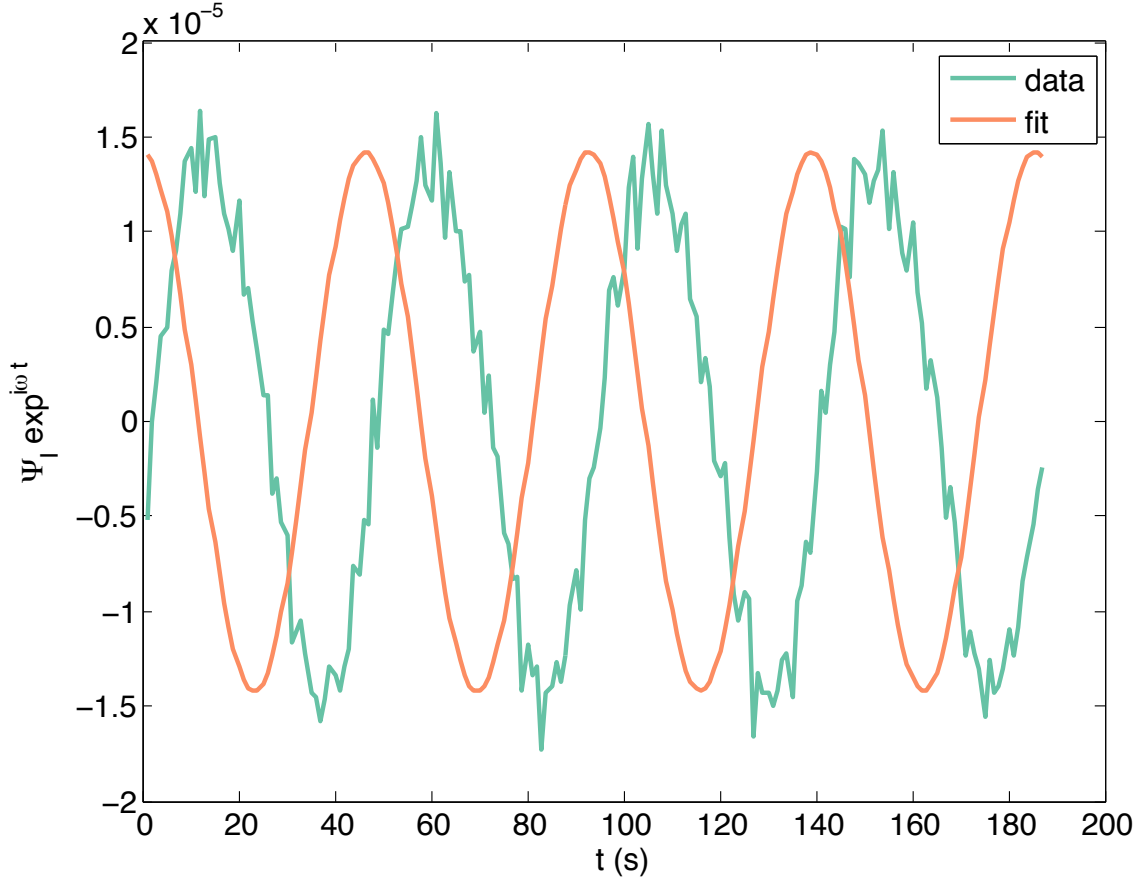
Figure 6: Comparison of velocities (arrows) and speeds (colours) in laboratory results (left) and theoretical model (right) for $\omega_0 = \omega_F = 0.1355\,\text{rad/s}$ at $f_0 = 3.1\,\text{rad/s}$ and $A_{\text{forcing}} = 2.0\,\text{cm}$.

273

Figure 7: Mean value of streamfunction around island and corresponding computed fit, $\Psi_I \cos \omega t$.

around the island at each point in time, which oscillates with frequency ω, and computing the root-mean-square velocity corresponding to this timeseries. An example of the data and corresponding fit for $\omega_0 = 0.1355 \, \mathrm{rad/s}$ and $A_{\mathrm{forcing}} = 2 \, \mathrm{cm}$ is shown in figure 7. Excellent agreement is seen between the amplitude of the oscillations in the experimental data and the computed amplitude Ψ_I.

A summary of the computed values of the island constant for all forcing frequencies and forcing amplitudes is shown in figure 8. Of note is the apparent lack of resonance, despite three of the forcing frequencies ($\omega_0 = 0.0690, 0.1010, 0.1355 \, \mathrm{rad/s}$) corresponding to the western subbasin, eastern subbasin, and full basin normal mode frequencies. This is particularly surprising given that the theoretical predictions of Pedlosky and Spall (1999)[8] and Pedlosky (2000)[5] indicate that resonant peaks should be observed in the value of Ψ_I (see, for instance, figure 4 of [5]).

An additional way in which the experimental results may be compared with the linear theory outlined above is by further examining the integral constraint defined in (25). We
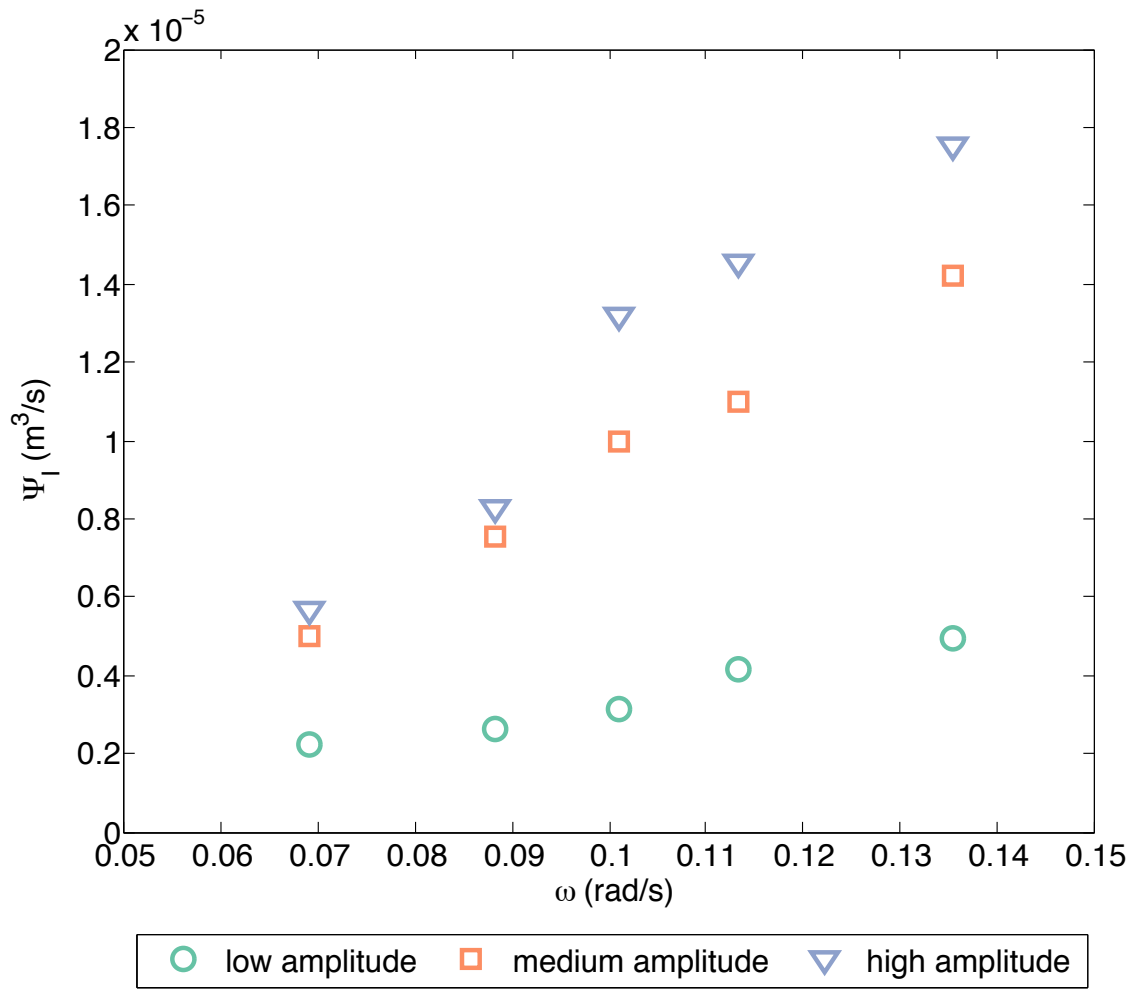
274

Figure 8: Computed values of island constant Ψ_I for different forcing frequencies and amplitudes.

redefine this expression as

$$\oint_{C_I} \mathbf{u} \cdot \mathrm{d}\mathbf{s} = \text{residual}. \tag{31}$$

By computing the individual components of the contour integral, the residual is determined.

The mean value of the computed residual is shown in figure 9, and the rms amplitudes of oscillation of each of the individual components of the contour integral are shown in figure 10. The amplitudes of the mean values are smaller than the rms amplitudes; however, it is clear from figure 10 that the amplitude of the residual value is comparable to that of some of the individual terms in the contour integral. This points to some missing physics in the contour integral. As the contour integral should be valid for nonlinear flows, the missing terms are likely related to missing viscous effects not accounted for in the linear theory (e.g. the assumption that lateral friction is negligible in the basin). This is, perhaps, unsurprising given that the laboratory's smaller length scales; viscous effects might be expected to be more dominant in the laboratory than at, say, geophysical scales.

4.3   Nonlinear effects

Figure 11 shows a zoomed-in view of the northern gap for $\omega_0 = 0.1134\,\text{rad/s}$ and $A_{\text{forcing}} = 2.7\,\text{cm}$. For these parameters, the scalings for nonlinearity in the basin and in the gaps are $NL_{\text{basin}} = 0.004$ and $NL_{\text{gap}} = 13.7$, respectively. As such, it is expected that significant nonlinear effects will be observed in the gap regions for these parameters.

Examination of figure 11 does show evidence of nonlinear effects. In particular, we can see the formation of a vortex on the western side of the barrier, and a strong boundary current on the eastern side of the barrier. Both the vortex and the strong east-west asymmetry are characteristic of strong nonlinear effects which are not well captured by the linear theory.

5   Discussion and conclusions

Here we have presented laboratory experiments corresponding to the theory of Pedlosky (2000)[5] and Pedlosky (2001)[6], which predicts that barriers with relatively small gaps may be quite inefficient in preventing the transmission of Rossby waves through the barriers. Comparisons between the linear theory and the experimental results indicate that the theory does capture the large-scale structure of the flow; however, preliminary analysis of the results points to the importance of additional physics not captured by the linear theory in its current form.

First, additional forcing frequencies would be of great interest, particularly to determine whether resonant peaks are seen in the laboratory experiments (as the linear theory suggests) or not. Given that only five frequencies were considered above, it may be the case that the resonant peaks were "missed" in some sense. On the other hand, if there is no evidence of resonance, it may be indicative of some additional physics not fully captured by the linear theory.

Modification of the forcing symmetry and/or the barrier symmetry and number of gaps would be of interest. Blocking off one of the gaps to confirm that only smaller-scale structures are able to pass through the gap would be of interest, as would adjusting the forcing
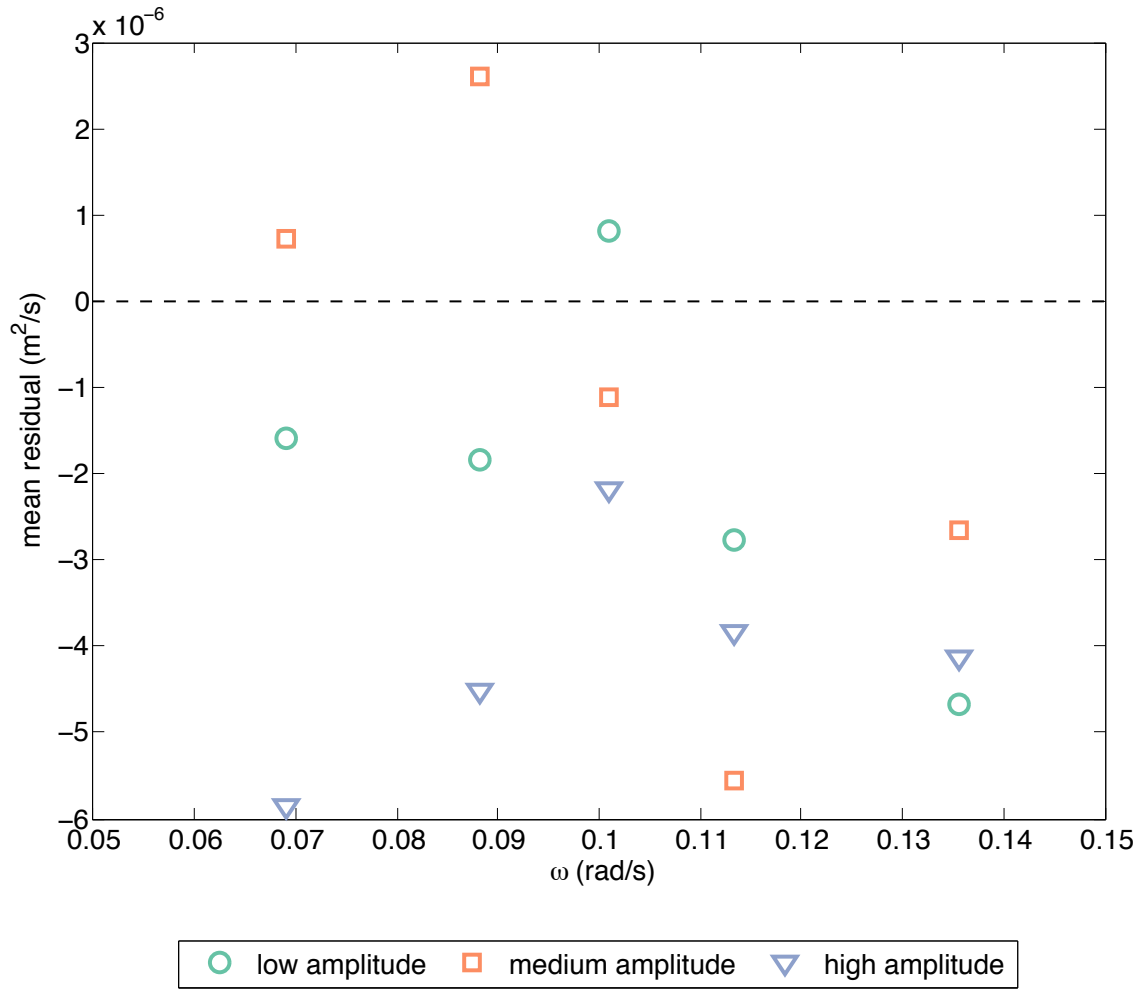
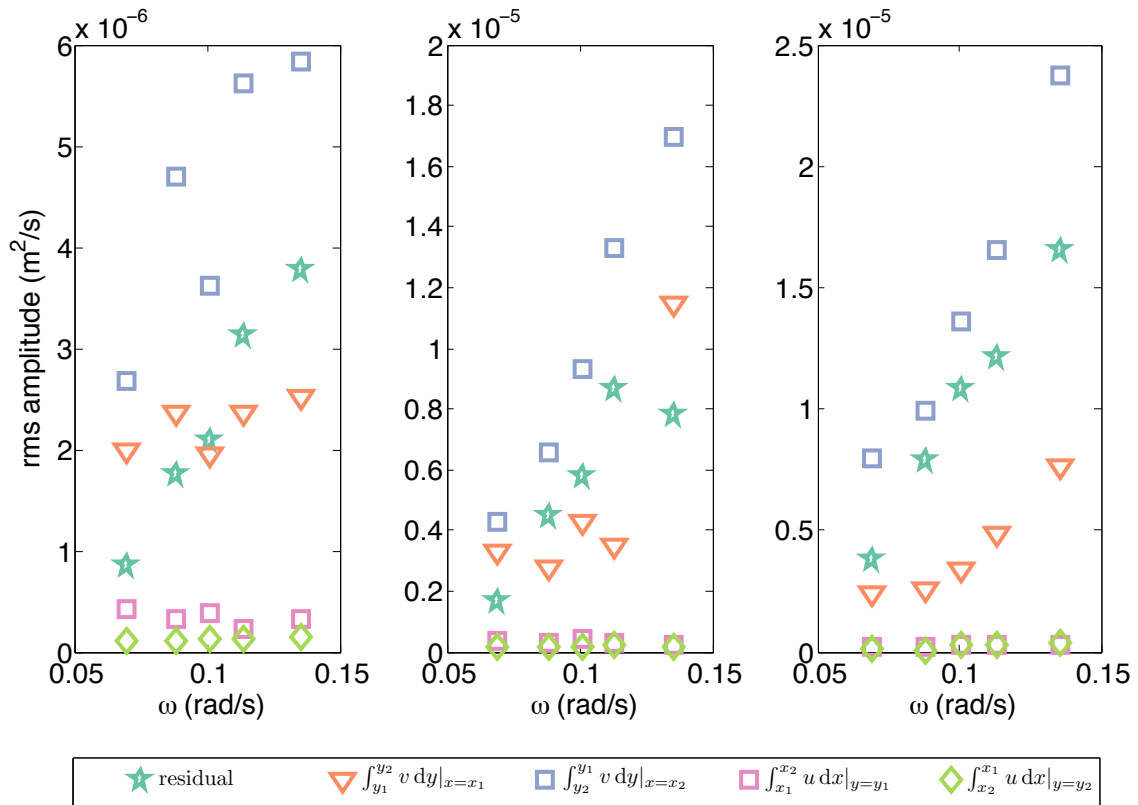Figure 9: Mean values of the computed residual from (31).

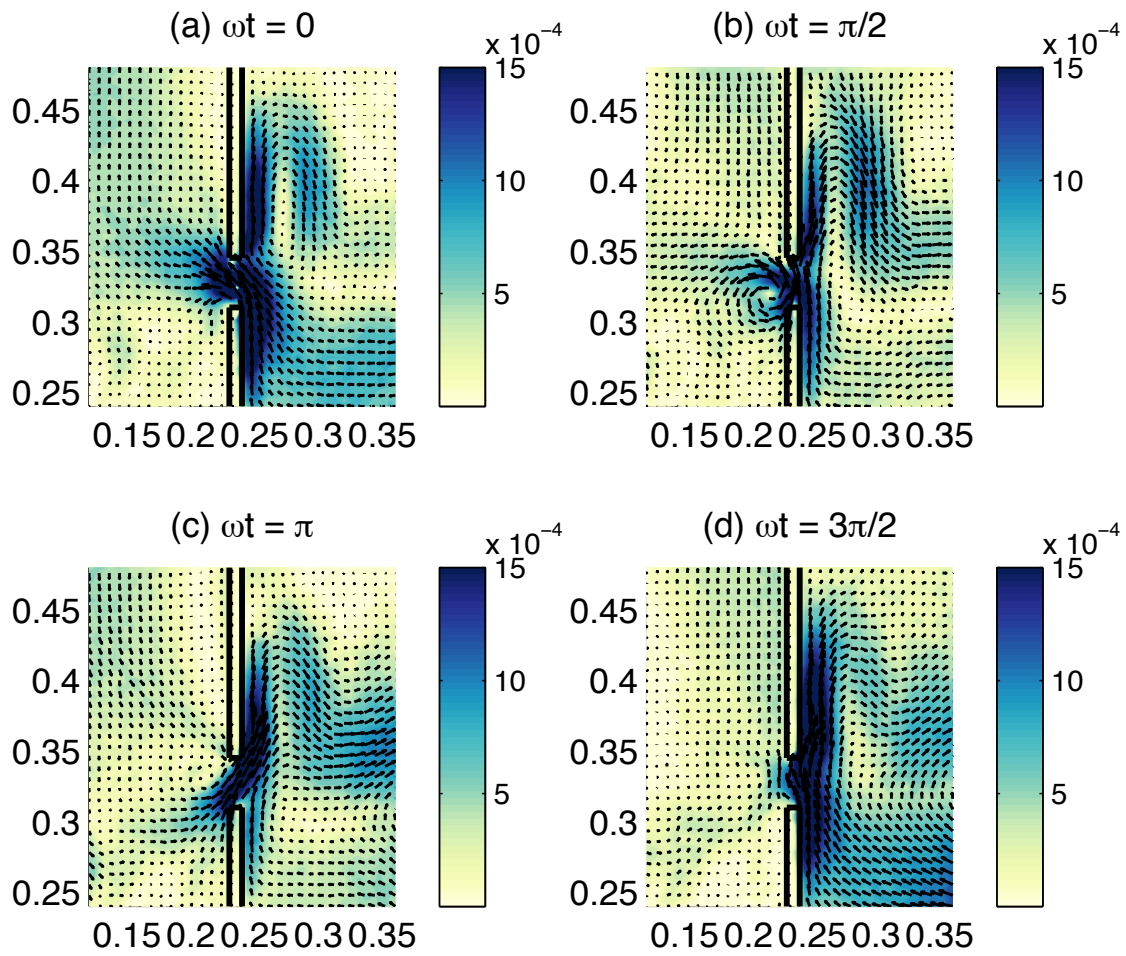Figure 10: Root-mean-square amplitudes of each term in (31).

Figure 11: Velocities (arrows) and speeds (colours) in laboratory results, zoomed in around the northern gap, for $\omega = 0.1134\,\mathrm{rad/s}$ at $f_0 = 3.1\,\mathrm{rad/s}$ and $A_{\mathrm{forcing}} = 2.7\,\mathrm{cm}$.

to one in which n is even. As Pedlosky and Spall (1999)[8] describe (see their figure 7), additional gaps in the barrier allow for different ways in which the waves may be transmitted through the barrier; comparing these scenarios with laboratory results could reveal further interesting features of the flow.

Additional forcing amplitudes could also be considered. In particular, it would be interesting to see if increasing the forcing could lead to separation of the vortex forming at the western side of the gap, shown in figure 11. Additionally, varying the forcing may help to quantify under what conditions these vortices form. As such vortices are an additional means by which wave energy may be transmitted into the western subbasin, and are a nonlinear effect not described by the linear theory described above, understanding their behaviour is of great interest.

Finally, numerical simulations corresponding to the laboratory length scales would be of great interest. In particular, while it is difficult to compute contributions due to viscosity from the measured velocities, owing to the noisy nature of the data and the higher derivatives that appear in viscous terms, these terms could be more easily computed from numerical data. This may help in quantifying the effects of nonlinearity and viscosity suggested to be of some importance by the experimental results.

6 Acknowledgments

References

[1] K. A. Kelly and L. Thompson, *Scatterometer winds explain damped Rossby waves*, Geophys. Res. Lett., 29 (2002), pp. 52–1–4.

[2] M. S. Longuet-Higgins, *Planetary waves on a rotating sphere*, Proc. Roy. Soc. A, 279 (1964), pp. 446–473.

[3] J. Pedlosky, *A study of the time dependent ocean circulation*, J. Atmos. Sci., 22 (1965), pp. 267–272.

[4] ——, *Fluctuating winds and the ocean circulation*, Tellus, 19 (1967), pp. 250–257.

[5] ——, *The transmission of Rossby waves through basin barriers*, J. Phys. Oceanogr., 30 (2000), pp. 495–511.

[6] ——, *The transparency of ocean barriers to Rossby waves: the Rossby slit problem*, J. Phys. Oceanogr., 31 (2001), pp. 336–352.

[7] J. Pedlosky, L. J. Pratt, M. A. Spall, and K. R. Helfrich, *Circulation around islands and ridges*, J. Mar. Res., 55 (1997), pp. 1199–1251.

[8] J. PEDLOSKY AND M. A. SPALL, *Rossby normal modes in basins with barriers*, J. Phys. Oceanogr., 29 (1999), pp. 2332–2349.

[9] B. A. WARREN, T. WHITWORTH III, AND J. H. LACASCE, *Forced resonant undulation in the deep Mascarene Basin*, Deep-Sea Res. II, 49 (2002), pp. 1513–1526.